Ain Shams Engineering Journal 15 (2024) 102596

Contents lists available at ScienceDirect

Ain Shams Engineering Journal

journal homepage: https://www.sciencedirect.com

Horizontal-axis propeller hydrokinetic turbine optimization by using the response surface methodology: Performance effect of rake and skew angles

Fredys Romero-Menco [a], Johan Betancour [a], Laura Velásquez [a], Ainhoa Rubio-Clemente [a,b], Edwin Chica [a,*]

[a] Grupo de Energía Alternativa, Departamento de Ingeniería Mecánica, Facultad de Ingeniería, Universidad de Antioquia, Calle 70 No 52-21, Medellín 050010, Colombia
[b] Escuela Ambiental, Facultad de Ingeniería, Universidad de Antioquia, Calle 70 No. 52-21, Medellín 050010, Colombia

ARTICLE INFO

Keywords:
Computational simulation
Experimental scaled model test
Optimization procedure
Prototype extrapolation
Renewable energy system
Water energy harvesting

ABSTRACT

The design of a horizontal-axis propeller hydrokinetic turbine (HPHT) depends on several geometric parameters affecting its hydrodynamic efficiency which is measured through the power coefficient (C_P). In this study, a 1 kW turbine with 1.6 m of rotor diameter (D) was used as the prototype to know the relationship between the C_P and the turbine design parameters, such as the skew (ϕ) and rake (γ) angles. A full-factorial design of experiments, as a response surface methodology technique, and computational fluid dynamics simulation were used to determine the significance of the factors considered and their interaction in the maximization of the response variable (C_P). A 3D computational domain in ANSYS Fluent software and the k-ω SST turbulence model were utilized, for the unsteady flow simulations. Under optimal design conditions, i.e., when ϕ and γ were equal to 13.30° and -18.06°, respectively, the highest C_P was 0.4571. For these optimal values, a scaled model with 0.24 m of diameter was numerical and experimentally studied and the findings were compared. A good agreement was found between the numerical results regarding the lab-scale turbine and the experimental data for the C_P values obtained as a function of the tip speed ratio.

1. Introduction

The United Nations (UN) has defined a list of purposes for humankind development having as its main objective the construction of a more just and equitable world [25]. Among these, guaranteeing environmental sustainability is highlighted, considering this goal as a transversal objective to the others. For this purpose, it is important to develop technologies that allow the use of clean, affordable, and safe energetic sources to supply the world's growing demand for energy and limit the increase in the average temperature of the planet below 1.5 °C [18,51]. The harnessing of hydrokinetic energy, as well as the development of hydrokinetic turbines, is a topic in which a lot of researchers are making contributions, mainly because the hydrokinetic systems do not require the construction of expensive civil works unlike the conventional hydropower plants [19]. This is an advantage both in economic and ecological terms and makes the preservation of the fauna and flora nearby for the hydrokinetic power plant installation to be possible.

The use of the kinetic energy of river or marine currents involves two processes. The former implies the transformation of the kinetic energy from the water flow energy to rotational energy in the turbine rotor. The latter refers to the conversion from rotational mechanical energy to electricity, which occurs in an electric power generator [50]. Most of the researches concerning the development of hydrokinetic turbines have been focused on the first process due to a general agreement about the optimal design of the blades is still absent [16]. Up to date, these elements have been designed considering procedures used to design wind generators as a reference [22], instead of having design methods properly developed for marine devices to act as a propeller, which had been traditionally used to give propulsion to water vehicles and whose principle is the same as a turbine but in a reverse way. Innumerable investigations with a significant contribution to the hydrokinetic turbine technology development were carried out [47,26,43,41,52,1,6]. The researchers focus on improving the design to achieve a better conversion of the water kinetic energy to electric energy when the turbine shaft

* Corresponding author at: Grupo de Energía Alternativa, Universidad De Antioquia, Calle 70 No 52-21, Lab. 19-106, Colombia.
E-mail address: edwin.chica@udea.edu.co (E. Chica).

https://doi.org/10.1016/j.asej.2023.102596
Received 27 August 2023; Received in revised form 16 October 2023; Accepted 23 November 2023
Available online 11 December 2023

is coupled to the generator. In the case of horizontal-axis propeller hydrokinetic turbines (HPHT), the number of researches reported in the literature is more limited [26]. In turn, in the field of the propeller optimization, from the authors' knowledge, several studies have been highlighted. Brizzolara et al. performed a multi-objective optimization using a genetic algorithm for two propeller models, one of them with a duct. The referred authors developed a panel method for the prediction of the hydrodynamic propeller applicable to open or ducted propellers, that are also subjected to cavitation [9]. In turn, Mirjalili and co-workers carried out the multi-objective optimization of a propeller using a particle swarm optimization aiming to minimize and maximize the cavitation and the efficiency, respectively. They evaluated the influence of the number of blades and the rotational velocity in the propeller optimization process. The results showed that the best performance and the lowest cavitation were achieved for a 5-6 bladed propeller in a regimen of rotational velocity between 170 and 180 RPM [31]. Furthermore, Nouri et al. performed the multi-objective optimization of a dual propeller counterrotating, using the Kriging method, as a substitute model, and the genetic algorithm. The objectives of the process consisted of achieving the best propeller hydrodynamic performance, minimizing the torque, and thrusting the difference between both analyzed models [35]. In turn, Ebrahimi and collaborators conducted a multi-objective optimization of a propeller DTMB 4119 through the application of the genetic algorithm and its implementation with the limit element method [21]. The modifications for the propeller under study included the variations of the skew angle (ϕ), the rake angle (γ), the radius, the pitch-diameter and the chord-diameter distribution. The proposed optimization objectives were the hydro-acoustic and hydrodynamic propeller performance, with the purpose of finding the optimal combination of factors that would allow a greater operating efficiency of the propeller with the lowest level of noise caused. The authors developed a numerical code to evaluate the propeller performance and the noise level by applying the panel method, in which they included the solution of the equation of Ffowcks, Williams & Hawkings (FW-H) to predict the noise level. For the experimental runs, ten parameters belonging to four variables (ϕ and γ, and the chord- and pitch-diameter relationships) were considered. For the optimization process, they used the commercial genetic algorithm package included in Matlab software and the Pareto front was built, which in this case it was made up of eleven geometric models that met the process restrictions. After evaluating the geometries, the authors concluded that the considerable noise level reduction produced by the propeller is ascribed to γ values ranging from 8.14° to 12.05°, and ϕ between 31.52° and 39.74°. According to the authors' best knowledge, and their experience in the process of optimizing propellers for hydrokinetic application, it is required to study the effect of ϕ and γ, whose influence is unknown considering the information reported in the literature.

The literature review underscores the innovative approach taken in optimizing horizontal-axis propeller hydrokinetic turbines (HPHT). Traditionally, much of the work in this field relied on one-factor-at-a-time (OFAT) techniques, which have limitations. In contrast, this research advances turbine rotor optimization by utilizing design of experiments (DoE) integrated with a response surface methodology (RSM). This approach investigates the relationship between skew (ϕ) and rake (γ) angles and the resulting power coefficient (C_p). The advantages of employing DoE over OFAT are manifold. Firstly, it allows for the simultaneous evaluation of multiple factors and their interactions in a single experiment, significantly expediting results compared to the time-consuming nature of OFAT, which necessitates a series of independent experiments for each factor. Secondly, DoE examines various levels of each factor concurrently, facilitating a more thorough exploration of the design space and the discovery of optimal factor combinations that might be overlooked with OFAT. Thirdly, it minimizes experimental errors by conducting multiple experiments in parallel, reducing result variability and leading to more robust conclusions. Furthermore, DoE is adept at identifying interactions between factors, a crucial aspect often neglected in OFAT. Lastly, employing DoE conserves both time and resources, as it requires fewer experiments to achieve optimal results in comparison to the OFAT approach. This research marks a substantial advancement in the hydrokinetic turbine field, introducing a more efficient and comprehensive optimization method. It underscores the importance of considering multiple factors and their interactions, as well as the benefits of using DoE to thoroughly and effectively explore the design space. Furthermore, a laboratory-scale model of the optimized turbine prototype was manufactured in order to experimentally validate the behavior of the turbine in a hydraulic channel.

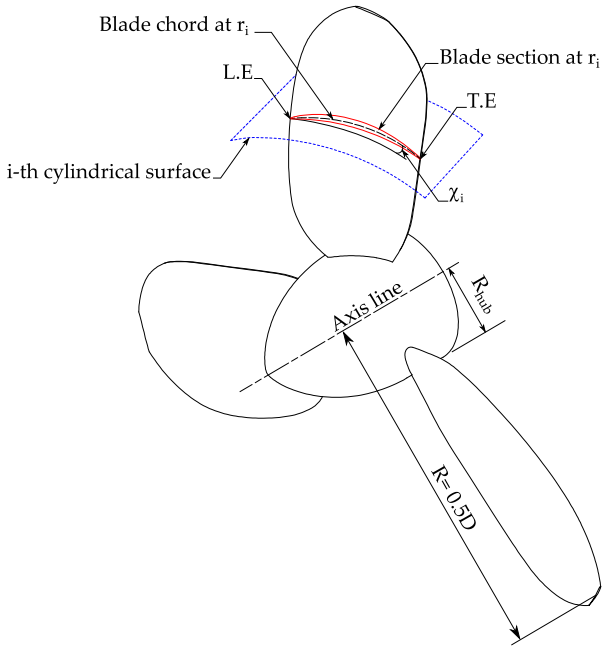

Fig. 1. Propeller hydrokinetic turbine. L.E is the foil leading edge. T.E is the foil trailing edge. r_i, is the radius at the i-th blade section. R_{hub} and R stand for the hub and the turbine radius, respectively. χ_i is the blade angle between the rotor plane and the local flow direction.

The paper comprehensively covers four main aspects in the following sections: (1) the design and calculation processes for turbine blades, (2) the careful selection of numerical simulation parameters, boundary conditions, and turbulence models, (3) the development of a mathematical model, and subsequent statistical analysis to comprehend the variation of C_p in relation to skew and rake angles, and (4) the crucial phase of experimental validation, coupled with the extrapolation of results to anticipate prototype performance

2. Methods and materials

2.1. Response surface methodology analysis

The complex geometry of the propeller is mainly characterized by several parameters, including the hub diameter (d), propeller diameter (D), number of blades (N), and the pitch angle (χ), among others. A distinctive feature of the propellers is that the sections of the profiles of the blades are defined on the surface of concentric cylindrical shells. Therefore, when the sections are projected on the surface, they acquire an oblique shape, as observed in Fig. 1. The propeller blades are defined with respect to a line perpendicular to the axis of rotation, commonly called the reference line or directrix. This line serves as a point to establish relationships, measurements and to locate characteristic points on the propeller blades [10]. For analysis purposes, the propeller is assumed to be a helicoidal surface, for which it is necessary to define three factors that determine the characteristic shape of the blades and their orientation. These parameters are χ, the skew or ϕ, and the rake

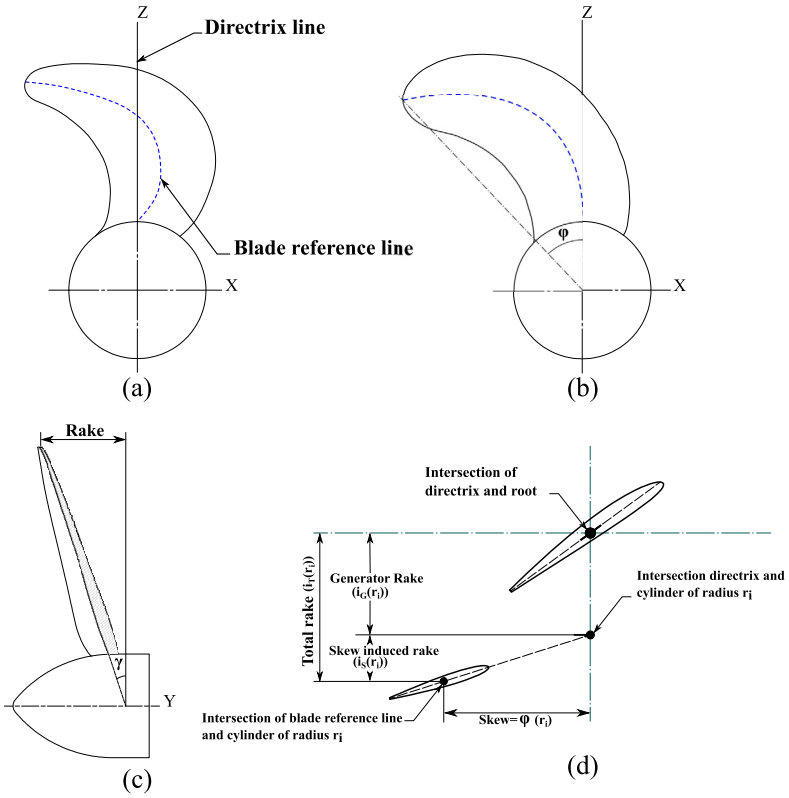

Fig. 2. Skew (ϕ) and rake (γ) in propeller blades. a) Balanced skew. b) Fully skewed skew. c) Angle section of the propeller blade rake. d) rake components.

or γ. The term χ is the orientation angle and refers to the helical advancement of the blades along a cylindrical surface [5]. ϕ is the angle formed between the directrix and the midpoint of the chord at a standardized non-dimensional distance x (r_i/R) [8]. There are two forms of obliquity known as balanced or biased. A balanced skew (Fig. 2a) where the position of the midpoints of the chords initially forwards from the guideline in the areas close to the hub, to later returns to be aligned with the guideline in areas close to the blade tip. In turn, the biased skew (Fig. 2b) occurs when the midpoint of the chord tends predominantly to be moved away from the guideline along the path of the blade [5]. γ is the angle that defines the inclination of the blade with respect to the axis line. Usually, this tilt is backwards (opposite direction to forward) to avoid contact between the propeller and the support elements. γ is divided into two components: the rake with respect to the directrix and the rake induced by the obliquity [10]. The latter is measured on a shear plane located at the center of the cube and is determined from the design stage, as illustrated in Fig. 2c. The rake induced by obliquity is the angle measured between the midpoints that are located between the chord of the first section and the chord of the tip section [5]. To better understand this difference, Fig. 2d explains graphically the composition of the total rake on the blades of a propeller.

During the design of a horizontal-axis propeller hydrokinetic turbine (HPHT), it is important to evaluate the effect of multiple factors and their simultaneous interactions on the studied variable to define the optimal treatment to minimize or maximize the desired response. For the case of the HPHT considered here, the selected factors were ϕ and γ. Concerning the response variable, the power coefficient (C_P) was considered. For defining the optimal value of ϕ and γ that maximize the turbine power generation, RSM and CFD approaches were used. The influence of several factors on the studied variable can be evaluated by using several designs of experiments (DoE). In this work, a full-factorial DoE was chosen to determine the combination of geometric factors aiming to maximize the C_P of the target HPHT. ϕ and γ were assessed as independent parameters for the DoE selected. The values of C_P were numerically calculated using the CFD of ANSYS Fluent software, which focused on URANS (incompressible unsteady Reynolds averaged Navier-Stokes) equations. The curve defined by representing C_P vs. TSR (tip speed ratio) values was constructed for the set of treatments. The C_P and TSR values are given by Eqs. (1) and (2), respectively.

$$C_P = \frac{P}{0.5 A \rho V^3} \tag{1}$$

$$TSR = \lambda = \frac{\omega R}{V} \tag{2}$$

where ρ is the water density; P stands for the turbine power output; A is the turbine cross-flow area, which can be calculated as the rotor swept area ($\pi D^2/4$); V is the water free stream velocity; ω stands for the turbine angular velocity; and R is the turbine radius. The value of P obtained from the CFD simulations can be written as expressed in Eq. (3)). In this equation, T represents the turbine total torsion.

$$P = T\omega \tag{3}$$

The horizontal-axis propeller hydrokinetic turbine (HPHT) prototype was designed to produce a P of 1 kW at 1.5 ms^{-1}. N and R were 3 and 0.82 m, respectively. The initial model of the HPHT is illustrated in Fig. 3. This model was designed by using the approach of the blade element momentum theory (BEMT). The referred theory is widely employed for the design of turbines and propellers [44,49,4,2,52].

In the combined momentum-blade element theory (CMBET), the propeller blade is divided into a finite number of sections along the blade span in a radial direction. In each one of these sections, a 2D force balance that involves lift and drag forces is applied. A set of equations is obtained, which can be solved iteratively for each blade cross-section, giving as results the values of the local chord ($C(r)$) and χ. The detail of the method is explained in depth by Schubel & Crossley [42] and Benini [4]. For the cross-section chord calculation, the Prandtl tip and the hub losses model corrections were used [7,43,49]. On the other hand, the distance of the section L.E to the directrix (d_r) was calculated to give

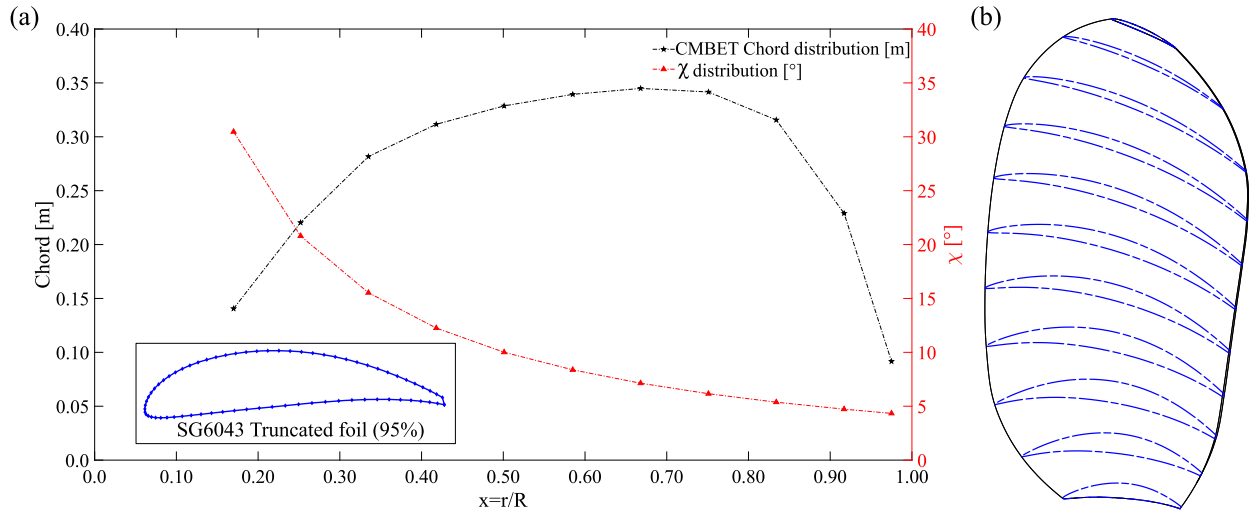

Fig. 3. Model of horizontal-axis propeller hydrokinetic turbine. (a) Twist angle and chord length distribution along the propeller blade obtained by the moment theory on the blade element and the foil used for the blade section. (b) CAD model of the blade designed initially. The blade cross-sections are displayed and the shape of the cylindrical surface that characterizes the propellers is showed.

the turbine blade the characteristic shape of a propeller using a curve fitting that determines this parameter as a function of the local chord value and the standardized distance x. The non-linear equation system to be solved in each section is described by Eqs. (4) - (10).

The propeller hub, can significantly impact the performance of a propeller due to its influence on the distribution of water flow around the blades. The design and dimensions of the hub can alter the way water flows to and from the propeller blades. This, in turn, can affect the efficiency of the propeller in generating thrust. For instance, a well-designed hub can reduce resistance and turbulence, resulting in smoother water flow over the blades and, therefore, higher thrust generation efficiency. In contrast, a poorly designed or inadequate hub can cause increased resistance and energy loss, ultimately decreasing the overall performance of the propeller. Therefore, investigating the effect of the hub on propeller performance is essential for optimizing its design and maximizing efficiency across various applications [17].

$$C(r) = \frac{8\pi V r_i^2 a'(1-a)F}{NW^2[C_L(\alpha)\sin\chi - C_D(\alpha)\cos\chi]} \tag{4}$$

$$W = \sqrt{V^2(1-a)^2 + \omega^2 r_i^2(1+a')^2} \tag{5}$$

$$F = F_{tip}F_{hub};\quad F_{tip} = \frac{2}{\pi}\cos^{-1}\exp^{\frac{-N(R-r_i)}{2r_i\sin\chi}};\quad F_{hub} = \frac{2}{\pi}\cos^{-1}\exp^{\frac{-N(r_i-R)}{2r_i\sin\chi}} \tag{6}$$

$$a'(1+a')\lambda_r^2 = a(1-a) \tag{7}$$

$$\lambda_r = \frac{\omega r_i}{V} = \lambda\frac{r_i}{R} \tag{8}$$

$$\tan\chi = \frac{(1-a)V}{(1-a')\omega r_i} = \frac{(1-a)1}{(1-a')\lambda_r} \tag{9}$$

$$d_r(x) = [-4.42x^5 + 10.36x^4 - 9.42x^3 + 3.79x^2 - 0.75x + 0.67]C(r) \tag{10}$$

where α refers to the blade angle of attack; C_D and C_L are the drag and lift coefficients of the foil, respectively. The values of these coefficients are a function of the α, which in turn is a function of the foil shape and performance. In this case, a group of 15 hydrofoils was compared using the *XFLR5* software, which facilitates the analysis of hydrofoils with a standardized unit chord length, allowing for meaningful comparisons [20]. The foils were compared in terms of the lift to drag ratio ($C_L(\alpha)/C_D(\alpha)$) in an α interval from 0° to 25°. Among the group of foils, the SG6043 foil was chosen due to the better performance exhibited ($C_L(\alpha)/C_D(\alpha)$ =169.81 at a α value of 2°). Likewise, W refers to the fluid relative velocity at the leading edge; F is the tip - hub losses factor; a and a' are the axial and radial induction factors, respectively; and λ_r is the local tip speed ratio (TSR). Additionally, the values of the chord length obtained with Eq. (4) were multiplied for a size correction factor (F_c) of 1.6, with the objective of improving the structural resistance of the blades considering the stresses on the blades during the operation [15]. Finally, for the blade shape definition and the geometric modifications introduced for ϕ and γ, the spatial coordinates of every superficial point of the blade were defined for Eqs. (11) – (13), according to the studies carried out by Klein and Morgan & Silovic [24,33].

Table 1
Geometric factors and levels involved in the optimization procedure of the horizontal-axis propeller hydrokinetic turbine.

Geometric factor	Values		
	-1	0	1
Skew angle (°), ϕ	0	15	30
Rake angle (°), γ	-20	0	20

(+1), (0) and (-1) refer to the high, central and low level, respectively.

$$X_p(r) = \{(x-d_r)\cos\chi - y\sin\chi\} + \left\{\left[\left(\frac{0.32}{\phi_{tip}} + \frac{\phi_{tip}}{2}\right) - \sqrt{\left(\frac{0.32}{\phi_{tip}} + \frac{\phi_{tip}}{2}\right)^2 - (r_i - 0.2)^2}\right]R\right\} \tag{11}$$

$$Y_p(r) = \{(x-d_r)\sin\chi + y\cos\chi\} \pm \{r_i\gamma\} \tag{12}$$

$$Z_p(r) = \sqrt{r_i^2 - \{[(x-d_r)\cos\chi] - y\sin\chi\}^2} \tag{13}$$

where ϕ_{tip} is the skew angle value at the blade tip; x and y correspond to the coordinates of the unit chord foil multiplied by the local chord length.

The initial geometry of the turbine was optimized considering ϕ and γ factors, as mentioned above. The effect of these factors was studied at +1, 0 and −1 that correspond to the high, medium and the low level, respectively, as listed in Table 1. The matrix domain was composed of 9 tests, which were randomly run. Finally, considering the data obtained from the simulation, regression models were developed. Eq. (14) describes the general expression representing the regression model built.

$$C_P = \beta_0 + \beta_1\phi + \beta_2\gamma + \beta_{12}\phi\gamma + \beta_{11}\phi^2 + \beta_{22}\gamma^2 \quad (14)$$

where, β_0 is a constant value; β_1 and β_2 correspond to the main effects of the geometric factors considered; β_{11} and β_{22} refer to the quadratic effect of the selected factors; and β_{12} stands for the interaction effects of the factors of interest on the response. Finally, C_P is the response variable.

ANOVA (analysis of variance) was utilized for the analysis of the numerical data found from the simulations. The application of this technique allows discerning the contribution of the studied parameters to the regression model [14]. To consider the possible errors, which are mainly due to the uncertainty conditions as the computer number representations, a significance level of 5% (0.05) was assumed. Therefore, to know the significance of an effect on the studied response, p-values are calculated.

On other hand, with the objective of evaluating the capability of the constructed model to explain the data that are not specified in the design space, a LoF (lack-of-fit) test was executed. The validation and adequacy of the model was calculated using R^2 and R^2_{adj}, representing the correlation coefficient and the determination coefficient adjusted by the degrees of freedom) [48,30]. Finally, 3D plots based on the behavior of the design factors in the experimental space and the C_P variation of the turbine as a function of the TSR were built. In the plots, the interactions between the response variable and the factors were investigated to obtain the combination of the factor levels that maximizes the response; i.e., the optimal treatment. For the data treatment and the statistical analysis, R Project for Statistical Computing software was used. The flowchart depicted in Fig. 4 provides a visual representation that clearly delineates the step-by-step optimization procedure explained in this section. In the presented flowchart, the first stage (P1) encompasses a comprehensive definition of the design requirements for a horizontal-axis propeller hydrokinetic turbine (HPHT), along with the identification of input parameters. The subsequent step (P2) involves intricate calculations for the propeller's geometry, including the chord length for each cross-sectional blade segment. Moving to the third phase (P3), the process delves into numerical simulation using CFD software to validate whether the rotor design aligns with the stipulated requirements, with a particular emphasis on spatial and temporal solution convergence analyses. In the fourth step (P4), the flowchart transitions to the geometric optimization process of the rotor, employing a response surface methodology and full factorial design. It's crucial to note that this phase includes a validation of assumptions to ensure the acceptability of the model representing the response variable in conjunction with the factors. This flowchart addresses the incidence of skew (ϕ) and rake (γ) angles on the performance of the horizontal-axis propeller hydrokinetic turbine (HPHT) within the scope of the study.

2.2. Numerical simulation

The influence of ϕ and γ on the horizontal-axis propeller hydrokinetic turbine efficiency was studied. For this purpose, CFD results were obtained using ANSYS Fluent software. Therefore, a computational domain, which consists of an internal and an external sub-domain, was required. A cylindrical shape was used for both sub-domains. The external sub-domain was a fixed cylinder with a length and a diameter of 9.375 D and 5 D, respectively. In turn, the turbine rotates in the internal domain, which has a length and a diameter equal to 0.625 D and 1.5 D, respectively. The rotor of the propeller was co-axially located to the cylinder axis and at 2.5 D from the inlet boundary conditions. 5a shows the main dimensions and the boundary conditions assigned. Uniform velocity, symmetry, no slip and pressure outlet were set as the inlet, external cylindrical surface, walls and outlet boundary conditions, respectively. 1.5 ms^{-1} was set as the uniform velocity inlet in the left boundary. In the y-axis direction, the gravitational acceleration and the outlet pressure were respectively set at 9.81 ms^{-2} and 0 Pa. The interfaces between the external and the internal domains were set by using the sliding mesh. The rotational velocity of the rotor was defined in the range from 0 RPM to 125 RPM, which is equivalent to a TSR range between 0 and 6.98. The mesh was generated using the ANSYS Fluent meshing module and a poly-hexcore mesh was built, mainly due to the advantages of using this mesh type, such as the computational time and the convergence improvement [46,45]. In Fig. 5, the computational domain and the meshed rotor 3D model are represented. Fig. 5b shows the polyhexcore mesh of the external domain. A refinement of the mesh downstream of the rotor was done to capture the vorticities caused on the flow. In Figs. 5c and 5d, the mesh of the internal domain and the mesh around the rotor, respectively, were illustrated. For the numerical analysis of the hydrokinetic turbine, the k-ω SST turbulence model was utilized. The referred model is preferably used because of its ability of predicting adverse pressure gradients in areas close to the wall and modeling properly the trail in areas far from it; thus, being able to predict an accurate turbine performance and a wake behavior [29,38]. The simulation was configured as a transient one.

In numerical studies, the estimation of the discretization error of the size mesh and the time step (Δt) is a transcendental part since they determine the adjustment and the concordance of the results; i.e., the numerical and experimental data fitting [11]. CFD software allows to solve a set of integral or differential equations describing the physical phenomenon governing the analyzed situation. However, the accuracy and precision of the results are linked to the size of the elements and the value of Δt used to describe the medium and time on which these equations will be solved [12]. A method widely used by several authors [41,11,38,39,36] for Δt and the mesh size convergence analyses of the solution is the use of the convergence index meshing (GCI) developed by Roache [40] and based on the Richardson extrapolation method. For the independence studies, three different time-steps and mesh densities were used. The solution estimation when the size of the elements approaches 0 is one of the advantages of this method. In addition, it allows to quantify the difference between the calculated asymptotic value and the numerical results [3]. The error estimation process using this method requires three successive refinements of the computational domain mesh (coarse (3), medium (2) and fine (1)) with a refinement factor (r) of at least 1.3 times the size of the previous mesh [12]. That is, the mean mesh must have at least 1.3 times the number of elements of the coarse mesh. Similarly, this relationship applies between the medium and the fine mesh. r can be determined as the ration between the medium mesh size and the characteristic size of the coarse mesh. This parameter can also be calculated by the ration between the size of the fine mesh and the characteristic size of the medium mesh. In turn, the GCI between meshes can be obtained by means of Eq. (15) when the fine and medium mesh solutions are used, or by means of Eq. (16) when the coarse and medium mesh solutions are used.

$$GCI_{1,2} = GCI_{fine} = \frac{F|\epsilon_1|}{r^p - 1} \quad (15)$$

$$GCI_{2,3} = GCI_{coarse} = \frac{F|\epsilon_2|}{r^p - 1} \quad (16)$$

where p is the convergence order, which is determined as expressed in Eq. (17). ϵ_1 is the estimated solution relative error of f (a control variable). f can be calculated as the difference between the fine (f_1) and the medium (f_2) solution divided by f_1. In turn, the difference between f_2 and the coarse solution (f_3) divided by f_2 allows to obtain ϵ_2. F is a safety factor, which is set at a value of 1.25 [11,12,28,27]. Nonetheless, other authors suggest that F must be defined according to the value obtained for p. For values contained in the interval $1.8 < p < 2.2$, a F value of 1.25 should be used. Therefore, for values located outside this interval, F will be 3 [36]. Accordingly, in this work, a F value of 1.25 was used. p was determined as expressed in Eq. (17).

$$p = \frac{\ln\left(\frac{f_3 - f_2}{f_2 - f_1}\right)}{\ln(r)} \quad (17)$$

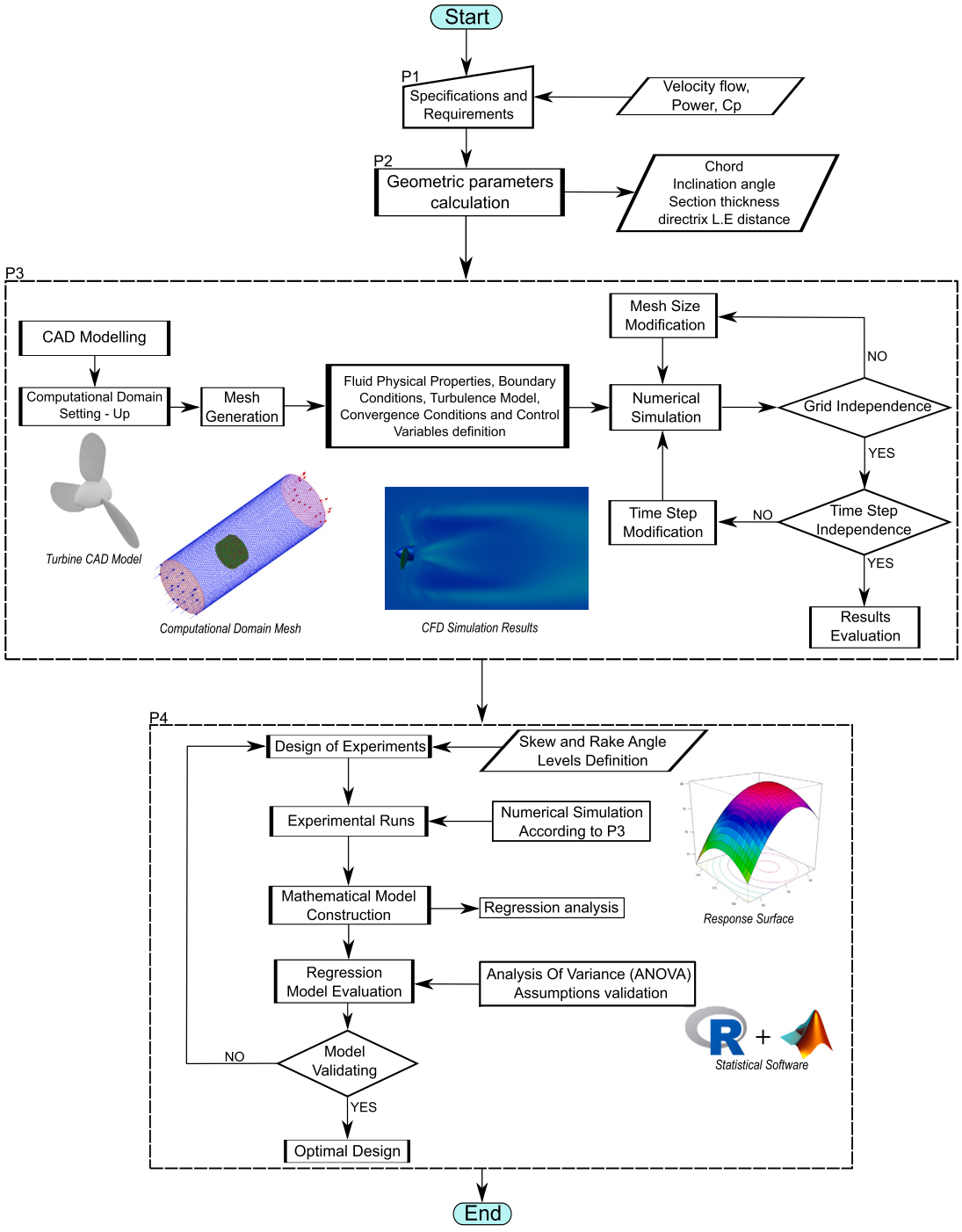

Fig. 4. Optimization methodology flowchart.

By knowing the value of p, it is possible to determine the analytical result of the asymptotic solution for a spacing value approx. 0 ($\Delta h \approx 0$). This solution will be given by Eq. (18) [11].

$$f_{h\approx 0} = f_1 + \frac{f_1 - f_2}{r^p - 1} \tag{18}$$

Finally, the convergence index asymptotic range (I) must be assessed to ensure that the mesh sizes and the time-steps selected are within the convergence asymptotic range. This variable is expressed by Eq. (19). Moreover, for the numerical simulation to be within the asymptotic range, I should approach 1.

$$I = \frac{GCI_{coarse}}{r^p GCI_{fine}} \approx 1 \tag{19}$$

The mesh size and Δt convergence analysis results for F equal to 1.25 are compiled in Table 2. To verify the mesh and time step independence, T was monitored. The independence tests were developed for a rotor rotational velocity of 107 RPM. As observed, the numerical results are independent on the mesh sizes and the time steps. In this regard, the medium time step and the medium mesh were selected to be used for the subsequent simulations. This decision was supported by the good compromise in terms of computational time and results achieved. In Fig. 6, the results from Richardson extrapolation for the mesh and time-step independence studies are shown. The values compiled in Table 1 correspond to the levels of the experimental treatments, on which further numerical simulation would be carried out to analyze the effect of factors on the hydrokinetic turbine. Fig. 7 shows some of the models

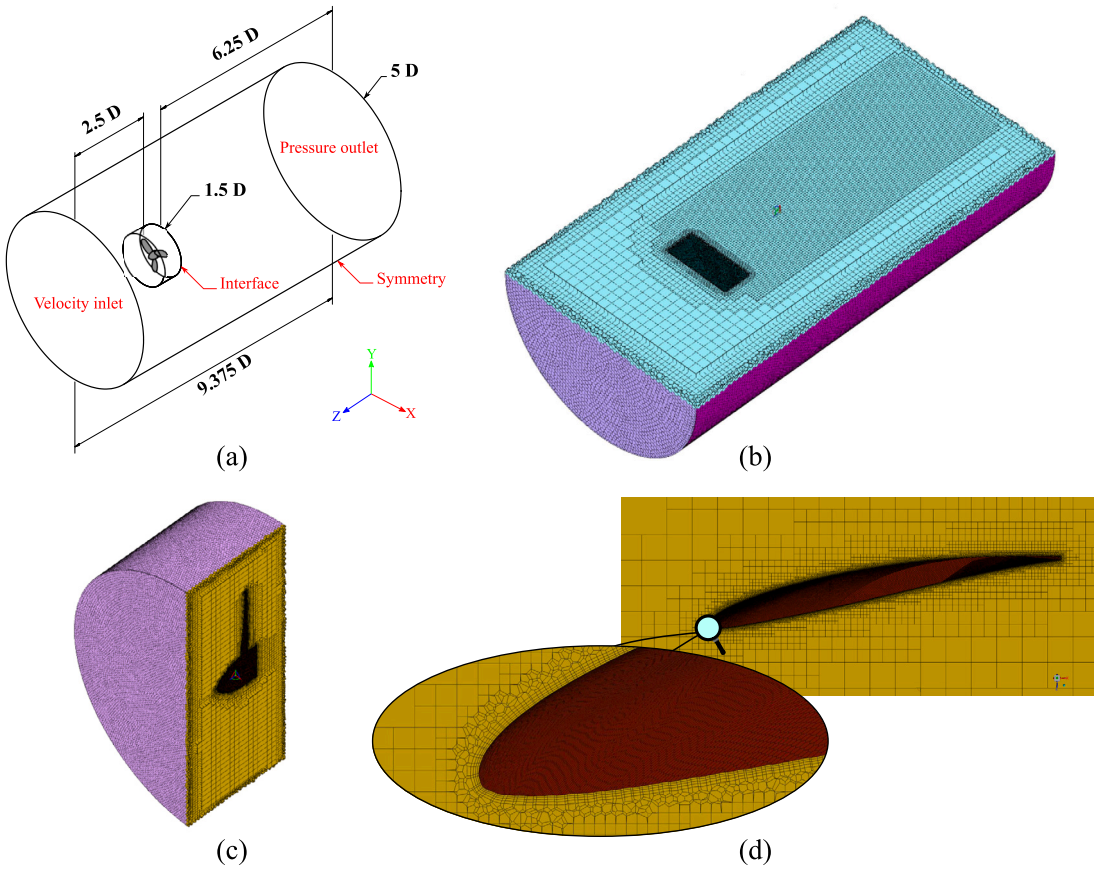

Fig. 5. Domain and mesh. a) Boundary condition setup and computational domain dimensions for ANSYS simulation. b) External domain mesh. c) Internal domain mesh. d) Mesh around the rotor. As it can be seen in the mesh, there are 4 boundary layers to capture the turbulent phenomena at the blade walls.

Table 2
Results from convergence analysis. The mesh and time independence results are listed at right and left, respectively.

$f = Torque\ [Nm]$						
	Number of elements			Time step (Δt)		
Fine (1)	5304055	f_1	86.21	0.0125	f_1	85.55
Medium (2)	2927011	f_2	85.65	0.025	f_2	85.75
Coarse (3)	1146692	f_3	76.32	0.05	f_3	86.21
		$GCI_{2,3}$	0.8695%		$TCI_{2,3}$	0.4470%
		$GCI_{1,2}$	0.0518%		$TCI_{1,2}$	0.0973%
		$f_{\Delta h \approx 0}$	86.35		$f_{\Delta t \approx 0}$	85.52
		I	1.0065		I	0.9983

used to assess the incidence of the factor different levels on the turbine C_P.

2.3. Experimental setup

The performance characterization of the horizontal-axis propeller hydrokinetic turbine (HPHT) scaled model was carried out. Fig. 8 shows the scaled model of the turbine with a rotor diameter (D) of 0.24 m, a ϕ and a γ equal to 13.30° and -18.06°, respectively. The model consisted of three blades, a shaft and a hub. The hub and the blades were economical and accurately manufactured by a 3D printing process. For the processing of polylactic acid (PLA), the fused filament fabrication (FFF) technology was used. The shaft was manufactured in AISI 304 stainless steel using conventional machining processes.

The experiments of the HPHT scaled model were carried out in an open hydraulic channel of 0.31 m width, 0.5 m height and 8 m length. To measure the water speed inside the channel, a flow-meter (FlowWatch FW450) was used, which had a velocity accuracy of ±0.01 ms^{-1}. An axial flow pump was used to drive the water that recirculates through the channel at a velocity of up to 1 ms^{-1}. The value of this velocity resulted to average the measurements of this variable at three different positions of the rotor upstream within the channel. The pump was controlled by a 14.9 kW electric motor. Fig. 9 presents an overview of the test facility. T and ω were measured using a sensor of the torque (Futek-Model TRS605) with encoder (accuracy of 0.000110 Nm and >10,000 C_pr, respectively). The sensor has a IHH500 pro intelligent digital display to monitor its activity, and the data obtained were saved in real time. For the measurement of the turbine T and ω, it was necessary to immerse the torque sensor and the data acquisition system in the water current in a submerged water-resistant vessel. In this regard, a water resistant vessel that would protect the sensor from the flow of water was constructed.

To measure the torque generated by the turbine at different TSR values, a braking system coupled to one end of the torque sensor was used. This system employs a direct current motor and a reverse current braking technique; i.e., an electric motor is used as a brake in the turbine model, which allows to keep the turbine model operation at a constant TSR. The technique consists of energizing the DC motor in the opposite direction to the turbine rotation, thus generating a torque in this direction (reactive), which reduces the turbine ω. In addition, the motor acts as an electric generator that is slowed down by the power demanded by the system. The braking torque is adjusted according to the desired turbine angular velocity (ω), so that the amount of current flowing to the DC motor is regulated by the pulse width modulation (PWM). In the developed system, it is achieved using a microcontroller and a power coupling circuit, which has the function of coupling the signal provided by the microcontroller with the power supply of the DC motor. When the turbine ω is required to be decreased (or increased), the microcontroller increases (or decreases) the work cycle of the PWM, and

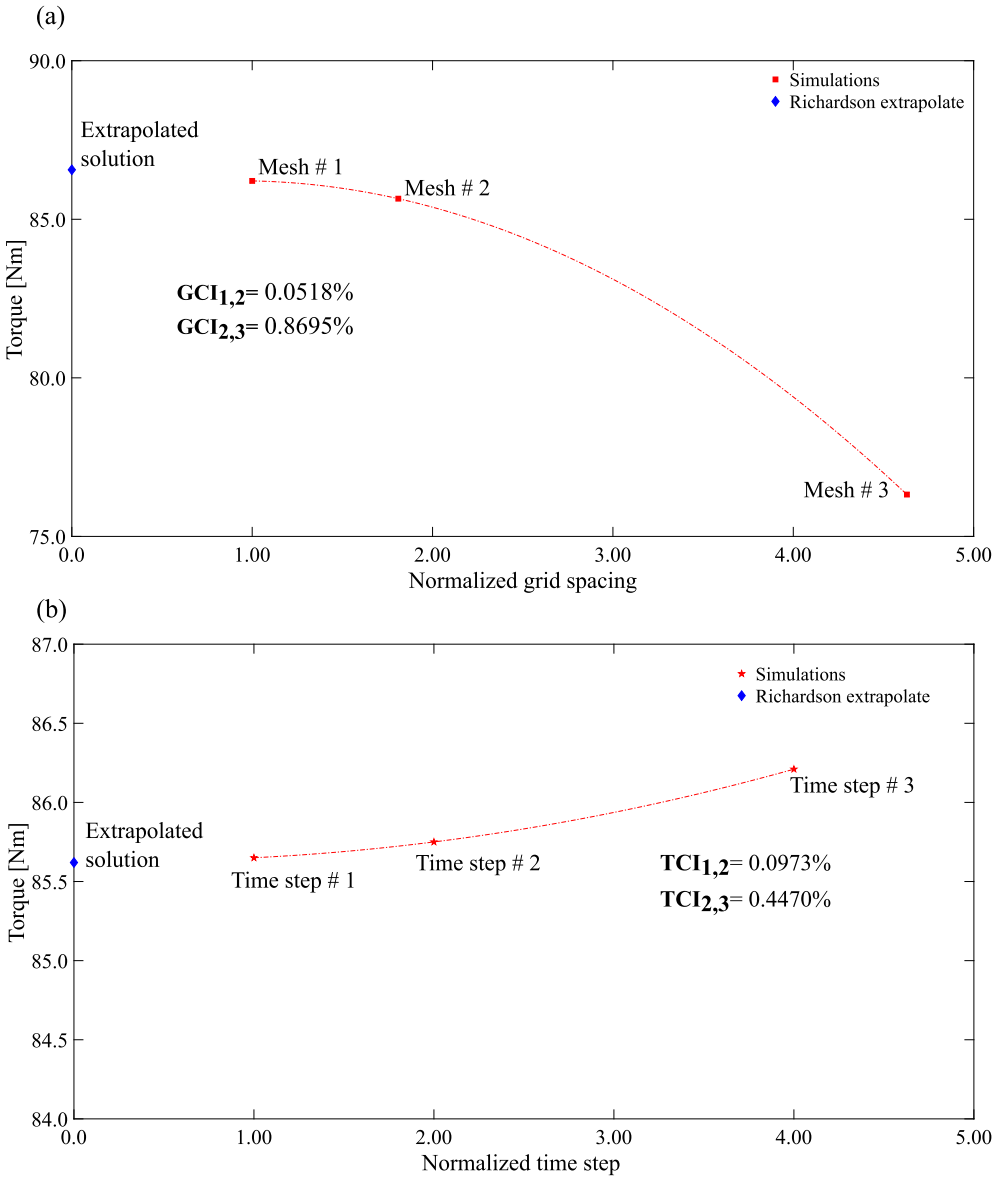

Fig. 6. Richardson extrapolation results. a) Mesh independence test results. b) Time independence test results.

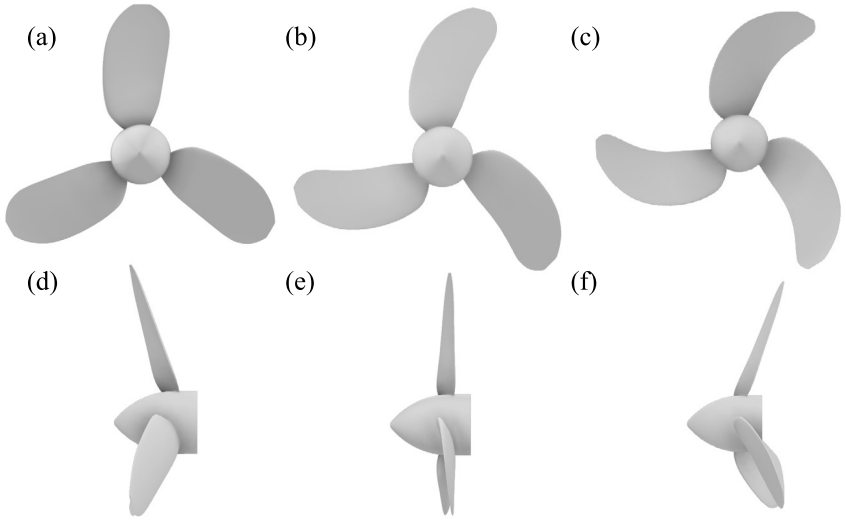

Fig. 7. CAD models of experimental units for the different levels of the factors. a) $\phi = 0^{\circ}$, b) $\phi = 15^{\circ}$, c) $\phi = 30^{\circ}$, d) $\gamma = -20^{\circ}$, e) $\gamma = 0^{\circ}$, f) $\gamma = 20^{\circ}$.

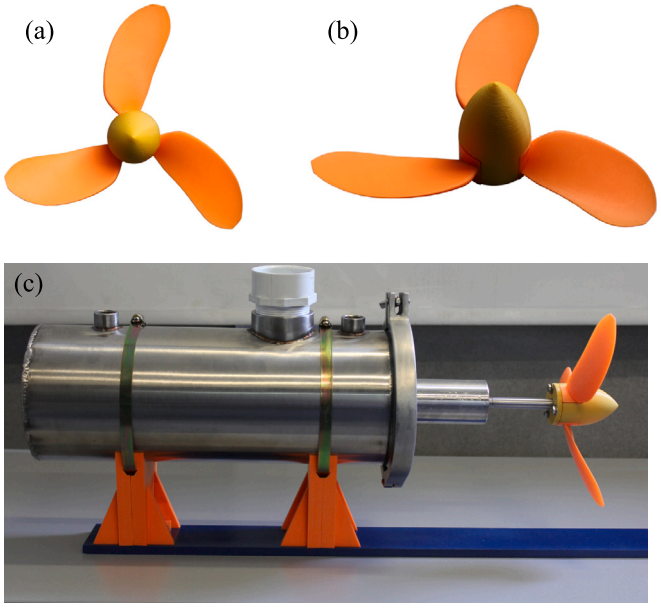

Fig. 8. Scaled model propeller hydrokinetic turbine. (a) Frontal view printed scaled model turbine. (b) Perspective view printed scaled model turbine. (c) Acquisition data assembly used in experimental tests.

subsequently, it increases (or decreases) the energy received by the engine. Consequently, the braking torque also increases (or decreases). To characterize the turbine model by means of a non-dimensional power performance curve that relates C_P to TSR, it was subjected to a uniform steady flow. Therefore, the rotor was perpendicularly aligned to the direction of the flow. The C_P values were calculated using Eq. (1). ~ 0.5 ms^{-1} was used as a fix value for the water free stream velocity and to achieve different TSR, ω was controlled.

3. Results and discussion

The C_P results as a function of TSR of 3 runs and the optimal geometric configuration are represented in Fig. 10. The maximal C_P was obtained from the treatment 6. The C_P maximal value was 0.4432 at a TSR equal to 3.6280 ($\sim$ 65 RPM) and a water velocity of 1.5 ms^{-1}. From the numerical results, the maximal C_P value was found for each treatment in order to perform the statistical analysis of the DoE conducted. The maximal values of C_P are shown in Table 3. The first analysis considered all factors and their interactions.

The model has a high R^2_{adj} (98.71%) and a p-value of 0.0049 ($<$ 0.05). Therefore, the quadratic regression model described by Eq. (20) represents the maximal C_P in a high significant way.

Table 3
Numerical and predicted responses for the full-factorial design matrix.

Treatment	Geometric factor		Power coefficient C_P		Error (%)
	Skew angle ϕ (°)	Rake angle γ (°)	CFD results	Predicted results	
1	0	0	0.4389	0.4393	0.0400
2	15	0	0.4454	0.4477	0.2300
3	30	20	0.4280	0.4299	0.1900
4	0	-20	0.4550	0.4542	0.0800
5	15	20	0.4279	0.4257	0.2200
6	30	-20	0.4432	0.4440	0.0800
7	30	0	0.4470	0.4443	0.2700
8	0	20	0.4094	0.4097	0.0300
9	15	-20	0.4550	0.4570	0.2000

$$C_P = 0.4393 + 9.505 \cdot 10^{-4}\phi - 1.112 \cdot 10^{-3}\gamma + 2.530 \cdot 10^{-5}\phi\gamma - 2.610 \cdot 10^{-5}\phi^2 - 1.841 \cdot 10^{-5}\gamma^2 \quad (20)$$

The results obtained from the ANOVA are presented in Table 4. According to these results, for the defined significance level of 0.05, most of the variables have a significant incidence on the regression model. However, the quadratic term of ϕ has a p-value slightly higher than the level of significance. Nonetheless, since it is a main factor, it was not removed from the model. Additionally, it is observed that γ has the greatest effect on the response variable, as it is the factor with the lowest p-value associated. These results are in agreement with those reported by Hayati et al. [23] for the thrust coefficient in the propellers. Based on Eq. (20), the C_P optimal value was determined, resulting to be 0.4571 when ϕ and γ were equal to 13.30° and -18.06°, respectively. In Fig. 11, the response surface obtained is illustrated.

After determining the most appropriate model to express the behavior of the C_P and having built the mathematical expression that relates the independent factors and the C_P values, the validation process was carried out for the regression assumptions. As commonly known, the regression must satisfy a set of hypotheses to guarantee the correct application of this model to the phenomenon studied [34]). In the specific case of the constructed regression model, the following assumptions were analyzed: i) correct specification of the model; ii) normality of residuals; iii) no autocorrelation of residuals (independence); and iv) constant variance of residuals (homoscedasticity). The tests used to verify that the assumptions are met do not actually quantify a level or degree of measurement at which the assumptions are met (since these are generally accepted). The first assumption (i.e., the correct model specification) is useful to verify whether during the model construction the variables that contribute to the variation of the response have been adequately considered [37]. For this specific case, the test determines if ϕ and γ have a contribution to the variation of C_P. To validate this assumption, Ramsey rest test was applied to the regression model and the p-value obtained was contrasted with 0.05, which

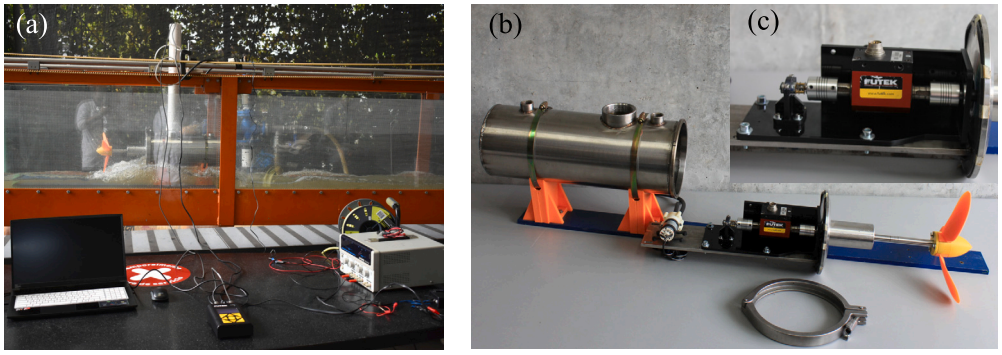

Fig. 9. Experimental setup of the recirculating water channel. (a) Experimental facility used in tests. (b) Experimental vessel and acquisition system set up. (c) Assembly torque sensor, DC motor and mechanical couplings.

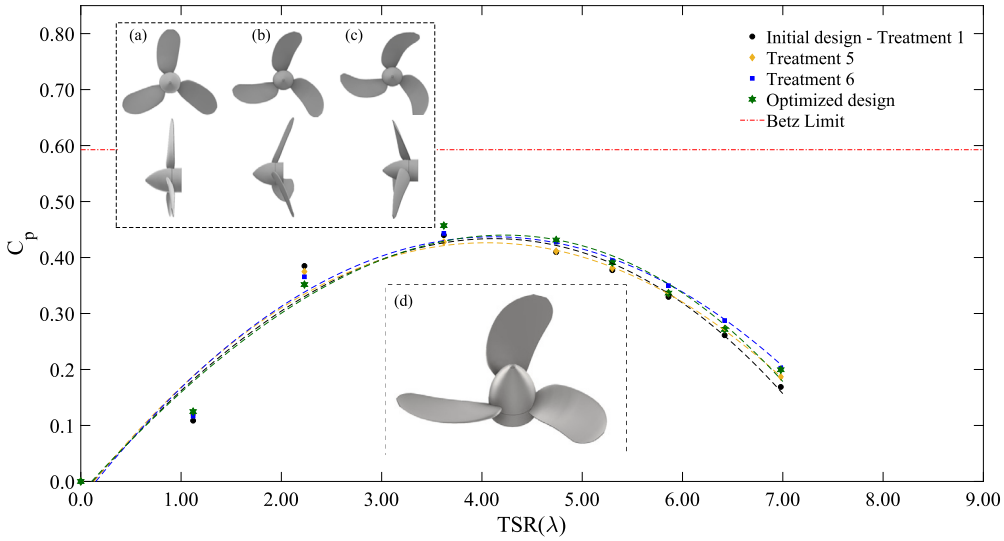

Fig. 10. C_P vs. λ for all the treatments and optimal design. The models (a), (b) and (c) correspond to the treatments used to validate the effect of the factors variation in the turbine performance. (d) Optimized turbine model with $\phi = 13.30^{\circ}$ and $\gamma = -18.06^{\circ}$.

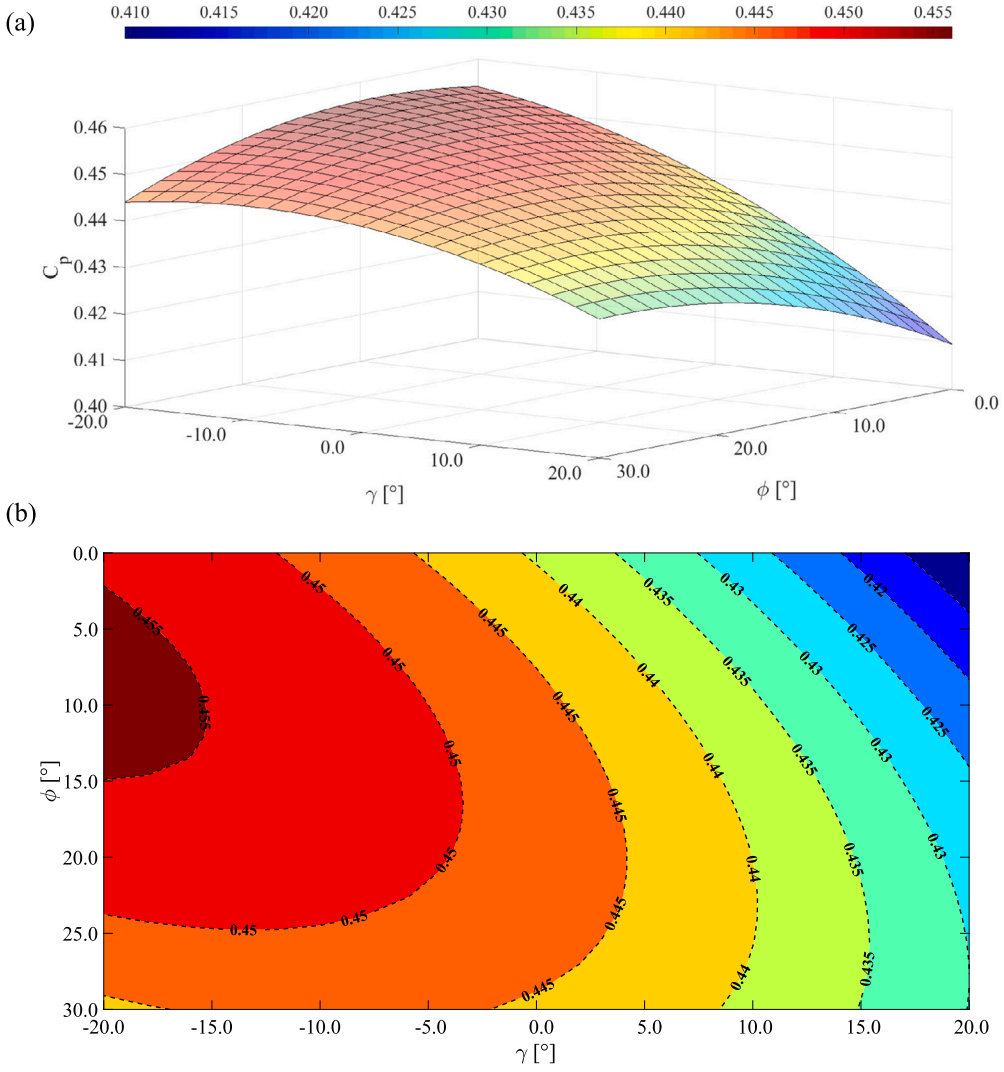

Fig. 11. Response surface plot related to the C_P showing the effects of the independent variables. (a) Surface 3D-plot. (b) Plant view surface and contour lines.

Table 4
Analysis of variance (ANOVA) for ϕ and γ.

Source of variation	Effect	Sum of squares (SS)	Degree of freedom (df)	Mean sum of squares (MS)	F-ratio	p-value
Model	–	0.0017340	5	0.0003468	45.88	$2.24*10^{-7}$
Skew angle, ϕ	$9.51*10^{-4}$	0.0000379	1	0.0000379	5.01	0.0388
Rake angle, γ	$1.11*10^{-3}$	0.0012884	1	0.0012884	170.43	0.0011
$\phi\gamma$	$2.53*10^{-5}$	0.0002304	1	0.0002304	30.47	0.0117
ϕ^2	$-2.61*10^{-5}$	0.0000689	1	0.0000689	9.12	0.0567
γ^2	$-1.84*10^{-5}$	0.0001084	1	0.0001085	14.34	0.0323
Error		0.0000226	3	0.0000076		
Total			8			0.0049

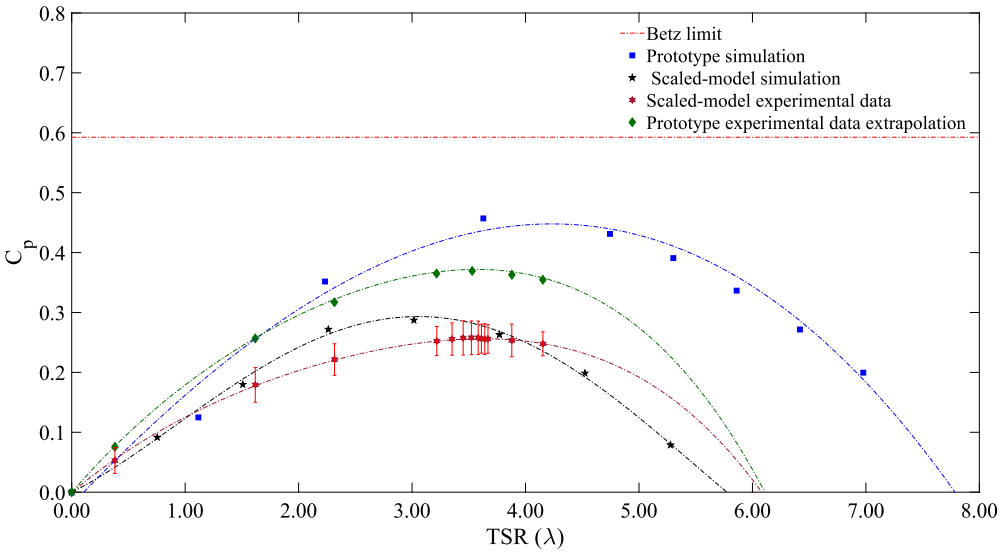

Fig. 12. Numerical and experimental comparison of C_P vs. TSR curves for scaled model and prototype.

is the value of the significance level as stated above. Here, the p-value obtained yielded a result of 0.6881; therefore, it was concluded that the model is correctly specified. With regard to normality, there are several tests that allow to verify this hypothesis. In this case, Jarque-Bera test was used, whose p-value was 0.6803; in this regard, the residuals are normally distributed. The independence of the residuals assumes that there is no a trend in their distribution. This assumption is strongly related to the principle of randomization of the runs [37]. To verify this hypothesis, Durbin-Watson test was used (p-value = 0.3824); thus the hypothesis of independence of the residuals of the constructed regression model was corroborated. Finally, homoscedasticity assumes that the treatments have the same variance; i.e., the variance is constant for all the residuals of the model [32]. The hypothesis to evaluate in this case is whether the variance is homogeneous. To verify it, Breusch-Pagan test was used. The test resulted in a p-value of 0.2256, so that the variance is accepted to be constant. According to the results presented, the regression model represented by Eq. (20) complies with the statistical assumptions, for which it is concluded that this equation can be used to predict the C_P behavior as a function of ϕ and γ.

In Fig. 12, the C_P vs. TSR values achieved from the CFD approach for the prototype and the HPHT scaled model are illustrated. Additionally, the experimental data for the scaled model are also presented. There is a difference between the results obtained from the simulations of the scaled model and those from the prototype. The difference in the C_P behavior becomes greater as the TSR value increases, which is due to the effect of the vorticities that has a higher incidence in smaller diameter models [13]. At a higher rotational velocity, the effect of the vortices at the tips are more evident (since the linear velocity acquires a higher value), thus affecting the overall performance of the scaled model. Regarding the comparison of the C_P values for the scaled model in experimental analysis, a displacement of the TSR is presented, at which the maximal value of C_P is reached. This difference is due to two fundamental reasons. The first one is the loss associated with the retainer seal used to prevent the water leakage inside the data acquisition set. The second reason corresponds to the influence of the blade surface roughness. Despite having obtained a good finish surface in the manufacturing process, the roughness influence on the performance of the turbine acquires a greater relevance as the size of the blades is smaller; that is, the relative roughness is greater. In the simulations, the blades were configured as walls without roughness, which allows for a smooth sliding of the fluid on the surface, reaching the values of C_P registered for the rotational velocity set. In the experimental case, the roughness peaks act as a resistance to the fluid flow on the surface of the blades due to the fluid viscosity. Therefore, to reach the same value of the relative velocity on the blade cross-sections, it is necessary to reach the same values of the forces causing the movement for the rotor to rotate at a higher velocity. The maximal C_P value of the prototype, the scaled model by the experimental tests and the scaled model by the numerical approach was found to be 0.4571, 0.2578 and 0.2871 at a TSR of 3.63, 3.5297 and 3.0159, respectively. In Fig. 12 the error bars are plotted for the scaled model data. The prototype extrapolated data presents a similar shape of the experimental scaled model, having a displacement of TSR.

Moreover, the experimental result extrapolation of the scaled model to the prototype can be seen in detail in Fig. 12. A Reynolds number (Re) correction was used to perform the referred transposition [7], which can be calculated as expressed by Eq. (21).

$$C_{P_{Prototype}} = C_{P_{Scaled-model}} \left(\frac{Re_{Prototype}}{Re_{Scaled-model}} \right)^{0.12} \quad (21)$$

Re can be calculated as showed in Eq. (22).

$$Re = \frac{\rho V R_C}{\mu} \quad (22)$$

where the dynamic viscosity is expressed as μ; R_C is equal to a characteristic chord length determined at a reference radial position (R_{ref}), which can be calculated as the average between the radius of the hub and the radius of the rotor. In the case of a propeller, a characteristic position that is usually used to describe the blade geometry is the radial position of 0.7 R, which is utilized to establish comparisons between different propeller models [10].

The experimental result extrapolation for the prototype and the numerical results are very close. This guarantees the blade design methodology achievement. The highest C_P was reached at the maximal value of 0.3693 (8.74% under the design C_P) at a TSR of 3.5297 (≈ 60 RPM).

4. Conclusions

In the work, the incidence of the skew (ϕ) and rake (γ) angles in the performance of a horizontal-axis propeller hydrokinetic turbine (HPHT) was determined. The optimization process was carried out through the RSM, which has been proven to be a powerful and practical technique for evaluating and analyzing the behavior of a system or process at a certain region of design. Additionally, a regression model was built to describe with a great precision the behavior of the turbine power coefficient (C_P) due to ϕ and γ variations. The results obtained from the optimization process showed that γ has a strong incidence on C_P. This is due to the fact that γ modifies the flow characteristics, mitigating the effects of the vortex at the blade tip. In addition, this geometric variation produces an increase in the pressure coefficient on both faces of the blade. The optimal value of γ was -18.06°. For the specific case of ϕ, it was found that the largest C_P was obtained in the range between 3 and 15°. The manufacture and characterization of a scaled model of a HPHT designed and optimized was carried out. The maximal C_P value for the scaled model simulations was 0.2871, which is slightly higher compared to the C_P reached experimentally (0.2878). Nevertheless, the displacement of the TSR at which the respective maximal values are reached is evident, being higher for the experimental results (3.5297) in comparison with the numerical ones (3.0159). The extrapolation of experimental results of the scaled model to the prototype has a good agreement with the results obtained in simulations and preserve the behavior observed in the scaled model.

List of symbols, abbreviations and acronyms

γ: Rake angle [°]
μ: Dynamic viscosity [kg m/s]
ω: Angular velocity [rad/s]
ϕ: Skew angle [°]
ρ: Water density [kg/m^3]
χ: Pitch angle [°]
α: Angle of attack [°]
A: Turbine sweep area [m^2]
C: Local chord length [m]
C_D: Drag coefficient [-]
C_L: Lift coefficient [-]
CFD: Computational fluid dynamics
C_p: Power Coefficient [-]
D: Rotor diameter [m]
d: Hub diameter [m]
d_r: directrix leading edge distance [-]
DC: Direct current
DoE: design of experiments
F_c: Size correction factor [-]
GCI: Grid convergence index
HPHT: Horizontal-axis propeller hydrokinetic turbine
N: Blades number [-]
OFAT: One factor at-a-time
P: Turbine power [W]
PWM: Pulse Width Modullation
R_c: Characteristic chord length [m]
R^2: Coefficient of determination [-]
R^2_{adj}: Coefficient adjusted of determination [-]
Re: Reynolds number [-]
RSM: Response surface method
T: Torque [Nm]
TCI: Time convergence index [-]
TSR: Tip speed ratio [-]
V: Water free stream velocity [m/s]
x: Non - dimensional distance [-]

CRediT authorship contribution statement

Romero-Menco, F: Writing – Original Draft, Writing – Review & Editing, Software, Investigation, Formal analysis, Validation, Visualization. **Betancour O, J:** Experimental Setup, Software, Formal analysis, Model fabrication. **Velásquez, L**: Validation, Methodology, Conceptualization, Data Curation, Formal analysis, Resources. **Rubio-Clemente, A:** Writing – Review & Editing, Visualization, Formal analysis, Methodology. **Chica, E:** Funding acquisition, Project administration, Writing – Review & Editing, Resources, Conceptualization, Methodology, Supervision.

Declaration of competing interest

The authors declare that they have no known competing financial interests or personal relationships that could have appeared to influence the work reported in this paper.

Acknowledgement

The authors thank the second joint call for I+D+i projects within the framework of the I+D→i regional agenda for the financial support provided to the project “Development of a propeller-type hydrokinetic turbine for the generation of electrical energy (in Spanish)”. Additionally, the authors acknowledge the financial support from University of Antioquia (Sustainability Strategy 2020-2021, ES84190067).

References

[1] Aguilar J, Velásquez L, Romero F, Betancour J, Rubio-Clemente A, Chica E. Numerical and experimental study of hydrofoil-flap arrangements for hydrokinetic turbine applications. J King Saud Univ, Eng Sci 2021.
[2] Amini H, Steen S. Experimental and theoretical analysis of propeller shaft loads in oblique inflow. J Ship Res 2011;55:268–88.
[3] Baker N, Kelly G, O'Sullivan PD. A grid convergence index study of mesh style effect on the accuracy of the numerical results for an indoor airflow profile. Int J Vent 2020;19:300–14.
[4] Benini E. Significance of blade element theory in performance prediction of marine propellers. Ocean Eng 2004;31:957–74.
[5] Bertram V. Practical ship hydrodynamics. Elsevier; 2011.
[6] Bouvant M, Betancour J, Velásquez L, Rubio-Clemente A, Chica E. Design optimization of an Archimedes screw turbine for hydrokinetic applications using the response surface methodology. Renew Energy 2021;172:941–54.
[7] Brasil Junior AC, Mendes RC, Wirrig T, Noguera R, Oliveira TF. On the design of propeller hydrokinetic turbines: the effect of the number of blades. J Braz Soc Mech Sci Eng 2019;41:1–14.
[8] Breslin JP, Andersen P. Hydrodynamics of ship propellers. 3. Cambridge University Press; 1996.
[9] Brizzolara S, Gaggero S, Grasso A. Parametric optimization of open and ducted propellers. In: SNAME 12th propeller and shafting symposium, OnePetro; 2009.
[10] Carlton J. Marine propellers and propulsion. Oxford, UK: Butterworth-Heinemann; 2018.

[11] Castedo R, Reifarth C, Santos AP, Losada J, López LM, Chiquito M, et al. Application of grid convergence index to shock wave validated with ls-dyna and prosair. Ing Investig 2019;39:20–6.
[12] Celik IB, Ghia U, Roache PJ, Freitas CJ. Procedure for estimation and reporting of uncertainty due to discretization in cfd applications. J Fluids Eng, Trans ASME 2008;130.
[13] Cengel YA, Cimbala JM, Sknarina SF. Mecánica de fluidos: fundamentos y aplicaciones. McGraw-Hill Interamericana; 2006.
[14] Chen WH, Wang JS, Chang MH, Mutuku JK, Hoang AT. Efficiency improvement of a vertical-axis wind turbine using a deflector optimized by Taguchi approach with modified additive method. Energy Convers Manag 2021;245:114609.
[15] Chica E, Rubio-Clemente A, Ismail B. Design of zero head turbines for power generation. London, UK: IntechOpen; 2017.
[16] Contreras LT, Lopez OD, Lain S. Computational fluid dynamics modelling and simulation of an inclined horizontal axis hydrokinetic turbine. Energies 2018;11:3151.
[17] Coşkun E, Doğru MH. Investigation of the hub diameter effect on propeller thrust. Int J Mater Eng Technol 2022;5:43–7.
[18] Cozier M. The 24th United Nations conference of parties (cop 24) climate change summit. Greenh Gases: Sci Technol 2019;9:6–9.
[19] Daskiran C, Riglin J, Schleicher W, Oztekin A. Transient analysis of micro-hydrokinetic turbines for river applications. Ocean Eng 2017;129:291–300.
[20] Drela M, Yungren H. Guidelines for xflr5 v6. 03 (analysis of foils and wings operating at low Reynolds numbers), 2011; 2018.
[21] Ebrahimi A, Seif MS, Nouri-Borujerdi A. Hydro-acoustic and hydrodynamic optimization of a marine propeller using genetic algorithm, boundary element method, and fw-h equations. J Mar Sci Eng 2019;7:321.
[22] van Els RH, Junior ACPB. The Brazilian experience with hydrokinetic turbines. Energy Proc 2015;75:259–64.
[23] Hayati A, Hashemi S, Shams M. A study on the effect of the rake angle on the performance of marine propellers. Proc Inst Mech Eng, Part C, J Mech Eng Sci 2012;226:940–55.
[24] Klein JL. A rational approach to propeller geometry. Technical Report. 1975.
[25] Laumann F, von Kügelgen J, Uehara THK, Barahona M. Complex interlinkages, key objectives, and nexuses among the sustainable development goals and climate change: a network analysis. Lancet Planet Health 2022;6:e422–30.
[26] Liu P, Bose N, Chen K, Xu Y. Development and optimization of dual-mode propellers for renewable energy. Renew Energy 2018;119:566–76.
[27] Mansour A, Laurien E. Numerical error analysis for three-dimensional cfd simulations in the two-room model containment thai+: grid convergence index, wall treatment error and scalability tests. Nucl Eng Des 2018;326:220–33.
[28] Meana-Fernández A, Fernandez Oro JM, Argüelles Díaz KM, Galdo-Vega M, Velarde-Suárez S. Application of Richardson extrapolation method to the cfd simulation of vertical-axis wind turbines and analysis of the flow field. Eng Appl Comput Fluid Mech 2019;13:359–76.
[29] Menter FR. Influence of freestream values on k-omega turbulence model predictions. AIAA J 1992;30:1657–9.
[30] Miliket TA, Ageze MB, Tigabu MT, Zeleke MA. Experimental characterizations of hybrid natural fiber-reinforced composite for wind turbine blades. Heliyon 2022;8:e09092.
[31] Mirjalili S, Lewis A, Mirjalili SAM. Multi-objective optimisation of marine propellers. Proc Comput Sci 2015;51:2247–56.
[32] Montgomery DC. Design and analysis of experiments. John Wiley & Sons; 2017.
[33] Morgan WB, Silovic V, Denny SB. Propeller lifting-surface corrections. Technical Report. Hydro-and aerodynamics lab lyngby (Denmark) hydrodynamics section; 1968.
[34] Myers RH, Montgomery DC, Vining GG, Robinson TJ. Generalized linear models: with applications in engineering and the sciences. John Wiley & Sons; 2012.
[35] Nouri NM, Mohammadi S, Zarezadeh M. Optimization of a marine contra-rotating propellers set. Ocean Eng 2018;167:397–404.
[36] Phillips TS, Roy CJ. Richardson extrapolation-based discretization uncertainty estimation for computational fluid dynamics. J Fluids Eng 2014;136.
[37] Pulido HG, De la Vara Salazar R, González PG, Martínez CT, Pérez MdCT. Análisis y diseño de experimentos. New York, NY, USA: McGraw-Hill; 2012.
[38] Riglin J, Schleicher WC, Oztekin A. Numerical analysis of a shrouded micro-hydrokinetic turbine unit. J Hydraul Res 2015;53:525–31.
[39] Riglin JD, Schleicher WC, Oztekin A. Cavitation phenomena and performance implications in Archimedes flow turbines. J Fluids Eng 2016;138.
[40] Roache PJ. Verification and validation in computational science and engineering, vol. 895. NM: Hermosa Albuquerque; 1998.
[41] Schleicher W, Riglin J, Oztekin A. Numerical characterization of a preliminary portable micro-hydrokinetic turbine rotor design. Renew Energy 2015;76:234–41.
[42] Schubel PJ, Crossley RJ. Wind turbine blade design. Energies 2012;5:3425–49.
[43] Siddappaji K, Turner MG. Revolutionary geometries of mobile hydrokinetic turbines for wind energy applications. In: Turbo expo: power for land, sea, and air. American Society of Mechanical Engineers; 2015:V009T46A009.
[44] Siddappaji K, Turner MG, Merchant A. General capability of parametric 3d blade design tool for turbomachinery. In: Turbo expo: power for land, sea, and air. American Society of Mechanical Engineers; 2012. p. 2331–44.
[45] Sosnowski M, Krzywanski J, Grabowska K, Gnatowska R. Polyhedral meshing in numerical analysis of conjugate heat transfer. In: EPJ web of conferences. EDP Sciences; 2018. p. 02096.
[46] Su J, Chai G, Wang L, Yu J, Cao W, Gu Z, et al. Direct numerical simulation of particle pore-scale transport through three-dimensional porous media with arbitrarily polyhedral mesh. Powder Technol 2020;367:576–96.
[47] Subhra Mukherji S, Kolekar N, Banerjee A, Mishra R. Numerical investigation and evaluation of optimum hydrodynamic performance of a horizontal axis hydrokinetic turbine. J Renew Sustain Energy 2011;3:063105.
[48] Taghinezhad J, Alimardani R, Masdari M, Mahmoodi E. Performance optimization of a dual-rotor ducted wind turbine by using response surface method. Energy Convers Manag X 2021;12:100120.
[49] Wang WQ, Yin R, Yan Y. Design and prediction hydrodynamic performance of horizontal axis micro-hydrokinetic river turbine. Renew Energy 2019;133:91–102.
[50] Yuce MI, Muratoglu A. Hydrokinetic energy conversion systems: a technology status review. Renew Sustain Energy Rev 2015;43:72–82.
[51] Yue Q, Wu H, Wang Y, Guo P. Achieving sustainable development goals in agricultural energy-water-food nexus system: an integrated inexact multi-objective optimization approach. Resour Conserv Recycl 2021;174:105833.
[52] Zhang K, Zou Q, Wang Y, Zhang B. Bionic shark fin combined airfoil blade optimal design and numerical simulation of horizontal axis tidal current turbine. Int J Energy Clean Environ 2017;18.

Fredys Romero-Menco: Mechanical engineer and research assistant at the University of Antioquia. Member of the research groups Energía Alternativa (GEA) and Manejo Eficiente de la Energía (GIMEL). He has research experience in areas related to the design and development of devices to use the renewable sources for power generation at small scale for off-grid systems. Likewise, he has been working in strategies for the reduction of pollutant emissions in biomass cookstoves. At industrial practice he has worked on operation and maintenance of hydroelectric power plants. He holds a master's degree in Mechanical Engineering (MsC) from University of Antioquia (Medellín, Colombia).

Johan Betancour Osorio: He holds a master's degree in Mechanical Engineering (MsC) from the University of Antioquia, with experience in research projects focused on energy generation through renewable and alternative sources. His primary focus has been on the development of new hydraulic systems for non-interconnected areas. He has also worked as professor in subjects related to hydraulics and alternative energies. Furthermore, he possesses industry experience in hydraulic and pumping system design, as well as in the design of gas and electrical appliances for cooking purposes.

Laura Isabel Velásquez García: She is a Mechanical Engineer graduated from the University of Antioquia (Medellín, Colombia). She holds a Master's degree in Engineering with an emphasis on Computational Mechanics from EAFIT University (Medellín, Colombia), as well as a Ph.D.'s degree in Environmental Engineering from the University of Antioquia (Medellín, Colombia). Currently, she serves as a professor at the University of Antioquia and a member of the research group Energía Alternativa (GEA). Within the GEA research group, she has contributed to the lines of hydraulic energy, hydrokinetic energy, wind energy, and wave energy. She has participated in research projects funded by MinCiencias and other university institutions. In these projects, she has been involved as co-investigator and principal investigator. As a result of these research efforts, she has published scientific articles in indexed journals and has participated in national and international conferences. As a researcher, her focus has been on the development and implementation of distributed renewable electricity generation systems, the study of turbulence phenomena, and computational fluid modeling. The majority of her current research applied mathematics, statistics, physics, computational simulations, and field and laboratory experiments to test new ideas and developments in the field of renewable energy.

Ainhoa Rubio-Clemente: Associated Professor at Environmental School of Faculty of Engineering of University of Antioquia, and a member of the research groups Diagnóstico y Control de la Contaminación (GDCON) and Energía Alternativa (GEA). She has teaching and research experience in areas related to the diagnosis of contamination of several environmental matrices, particularly water, as well as in their treatment through the implementation of alternative processes to those conventionally used nowadays. Likewise, she has participated in a number of research projects focused on the characterization of natural resources for their subsequent use as non-conventional sources of renewable energy. She holds a degree in Environmental Sciences (equivalent to level 3 of the MECES) from University of Salamanca (Salamanca, Spain), a master's degree in Bilingual Education from International University of La Rioja (La Rioja, Spain), a Ph.D.'s degree in Environmental Engineering from University of Antioquia (Medellín, Colombia) and a Ph.D.'s degree in Health Sciences from San Antonio de Murcia Catholic University (Murcia, Spain).

Edwin Lenin Chica Arrieta: Mechanical engineer and a full professor of Mechanical Department at Faculty of Engineering of University of Antioquia. He has teaching and research expertise in areas related to structural design and renewable energy from conventional and non-conventional renewable energy sources. He is the head of the research group Energía Alternativa (GEA) at University of Antioquia. He holds a Ph.D.'s degree in Industrial Engineering from University of Valladolid (Valladolid, Spain) complemented by a master's degree in Engineering and a specialization focused on Mechanical Design from EAFIT University (Medellín, Colombia). Among his research interest areas, the design of mechanical devices for the utilization of renewable energy sources, and the design of devices for water treatment, are included.